# Precipitation sequence in a QE22 magnesium alloy

G. Barucca,[1] A. Di Cristoforo,[1] D. Lussana,[2] P. Mengucci,[1] E. Santecchia[1]

[1]*Dipartimento di Fisica e Ingegneria dei Materiali e del Territorio, Università Politecnica delle Marche, Ancona, Italy*
[2]*Dipartimento di Chimica I.F.M., Centro di Eccellenza N.I.S. and CNISM, Università di Torino,Italy*

Corresponding author: Paolo Mengucci,
Dipartimento di Fisica e Ingegneria dei Materiali e del Territorio, Università Politecnica delle Marche,
Via Brecce Bianche, I-60131 Ancona, Italy
Tel. +39.071.2204733 Fax +39.071.2204729
E-mail: p.mengucci@univpm.it

**Summary**
The hardening phase evolution in a QE22 Mg alloy is followed by differential scanning calorimetry, microhardness and transmission electron microscopy, after different thermal treatments. The decomposition of the supersaturated solid solution occurs via the formation of nanometric coherent structures (co-clusters or GP zones) followed by the co-precipitation of two metastable phases responsible for the peak ageing condition. The stable phase $(Mg,Ag)_{12}Nd$ appears at the highest annealing times, giving rise to overageing and hardness reduction. TEM observations provide information on the crystallographic structure of the forming phases.

**Key words:** precipitation hardening, thermal treatments, differential scanning calorimetry, transmission electron microscopy.

## Introduction

The increasing demand of weight reduction in the automotive and aeronautical industry has renewed the interest in the study of magnesium alloys, despite its relatively high production costs. Magnesium is a good potential element for many structural applications, although the ageing response of magnesium alloys is not as relevant as that of aluminium alloys, but the addition of particular solute atoms has proved to increase the tensile properties as well as the hardness of several Mg-based compositions (Polmear, 2006). In particular, it has been shown that the addition of 2-3 wt.% Ag in rare-earth-containing alloys markedly improves their age hardening response and hence their mechanical properties (Payne and Bailey, 1959–1960). This paper studies the phase transformations occurring in a Mg–Nd–Ag–Zr commercial alloy (commonly named QE22) when submitted to different thermal treatments. QE22 is part of a series of alloys with tensile properties comparable with the high-strength aluminium casting alloys and it has been used for a number of aeronautical applications (Kannan *et al.*, 2008; Luo and Pekguleryuz, 1994). In this paper a structural analysis of the precipitation sequence in a QE22 magnesium alloy is reported. Investigations were carried out by differential scanning calorimetry (DSC) analyses, microhardness tests and transmission electron microscopy (TEM) observations.

## Materials and Methods

As-cast commercial QE22 bars with composition Mg–2.2Nd–2.1Ag–0.6Zr (wt%) were used. Slices about 1 mm thick were cut, from which small discs about 5 mm in diameter were obtained by punching. The discs were solution heat treated in a vertical furnace at 530°C for 6 hours, then quenched in water at room temperature. After this treatment they were stored at about -18°C in order to avoid phase transformations before performing annealing and analyses. The DSC measurements were carried out by a TA2010 calorimeter in a protective argon atmosphere. Pure Al with approximately the same weight as the sample (≈50 mg) was used as a reference. Thermal treatments were performed in an air-ventilated oven, at the highest temperature, or in a horizontal electrical furnace.

Microhardness tests were performed on the same samples used for calorimetric scans. Vickers hardness numbers were obtained with a load of 3 N by averaging at least five indentations.
TEM observations were performed at 200 kV with a Philips CM200 electron microscope equipped with a $LaB_6$ cathode. Samples were mechanically ground by emery papers, and an ultrasonic disc cutter (Gatan 601) was used to obtain discs with a diameter of 3 mm. The mechanical pre-thinning of a central area of each disc was performed by a dimple grinder (Gatan 656) while the final thinning was carried out in a precision ion polishing system (Gatan 691 PIPS) at 5 kV with the two guns at 4° of incidence.

## Results and Discussion

The DSC trace of the solution treated and water quenched (AQ) sample at a scanning rate of 5 $K \cdot min^{-1}$ is reported in Figure 1. As it is well known, the DSC technique is able to monitor phase transformations on scanning in temperature by revealing the specific heat variations due to atomic reorganization. At a first approximation, depletion of solute atoms from the out-of-equilibrium solid solution produces an exothermic peak of precipitation and vice versa for the endothermic signals.
In Figure 1, little can be said for the first part of the scan at low temperature, except for the formation of an endothermic signal D, positioned at ~200°C, following a region in which a broadened exothermic effect seems to be present. This implies that some aggregates, present just after quenching or developing during the scan at low temperatures, dissolve near 200°C, giving rise to the signal D.
TEM observations of the AQ sample, reported in a previous work, show a fine precipitation of nanometric structures uniformly distributed inside the grains (Barucca *et al.*, 2009). Although this precipitation is clearly visible in bright field images, it does not produce any remarkable effect on the diffraction pattern, suggesting a complete coherency of the nanometric structures with Mg. It is most probable that such nanometric structures are co-clusters or Guinier-Preston zones (Starink and Wang, 2009; Lambri and Riehmann, 2005; Polmear, 2006).
Above 200°C, three exothermic signals P1, P2 and P3 appear in Figure 1. The origin of these effects can be investigated by heat treating the samples at temperatures suggested by the signal positions.
Actually, the scan of the AQ sample in Figure 1 shows (also taking into account the thermal drag due to the scanning rate) that the temperature value of 204 °C is positioned just after the pre-precipitates dissolution peak (signal D) and before any appreciable subsequent precipitation signal. Therefore, the precipitation effects responsible of the signals P1 and P2 can be studied by ageing the alloy around that temperature (204°C). Furthermore, in order to fully characterise the entire precipitation sequence of the alloy, two more temperature values at 150°C (before the signal D) and 275 °C (just after the peak P2) were considered for the ageing treatments (Figure 1).
The calorimetric traces of the samples treated at 204°C for various ageing times are reported in Figure 2. Here, the progressive disappearance of

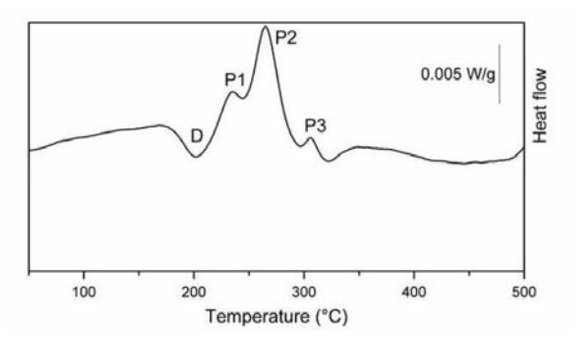


**Figure 1. DSC trace for the solution treated and water quenched (AQ) sample. Scanning rate: 5 K min$^{-1}$.**

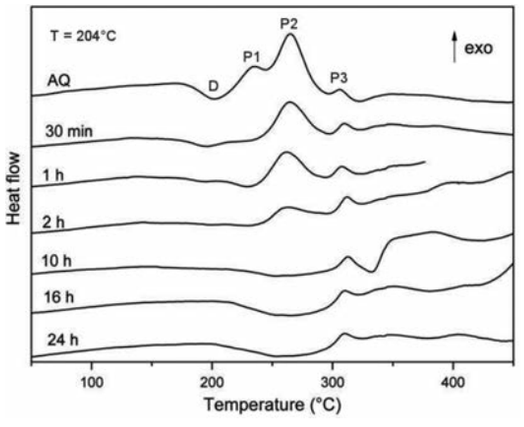


**Figure 2. DSC traces after ageing at 204 °C for the labelled times. Scanning rate: 5 K min$^{-1}$.**

the precipitation peaks P1 and P2, as well as the dissolution signal D at the increasing of the ageing time is clearly visible. In particular, it is worth to note that the sample aged for 10 hours at 204°C (ageing treatment T6) shows only the exothermic signal P3 corresponding to a precipitation effect. This means that during the thermal treatment at 204 °C the phases responsible for the precipitation peaks P1 and P2 were formed while the phase formation or transformation linked to the P3 signal did not occur.

The alloy hardness evolution on ageing at 150°C (triangles), 204°C (squares) and 275°C (dots) is reported in Figure 3. The error bar represents the standard deviation associated to each data point while the curves are only a guide for the eye.

The hardness evolution at 204°C confirms that, after 10 hours at this temperature, the peak ageing condition is reached, after which over-ageing occurs, leading to a decrease in hardness.

TEM observations of the sample in the T6 condition, performed in the $<001>_{Mg}$ zone axis orientation, reveal the presence of fine precipitates uniformly distributed inside the grains with dimension ranging from 10 to 50 nm, Figure 4a. The corresponding selected area diffraction (SAD) pattern of the sample is reported in figure 4b (upper part), together with the simulation (lower part) realized by the Crystal- KitX program (CrystalKitX software). Here, the most evident effect is the triangular structure located at $\sim 1/3\{-1-10\}_{Mg}$. This triangular arrangement of spots, as confirmed by the simulation, can be ascribed to diffraction from a secondary phase and to double diffraction effects. TEM observations performed under different orientations allow evaluating the lattice parameters of this secondary phase and its orientation relationships with the matrix. In the following, this secondary phase is referred to as the $\chi$ phase. Results show that the $\chi$ phase is hexagonal with a=0.286 nm and c=0.521 nm, and it precipitates

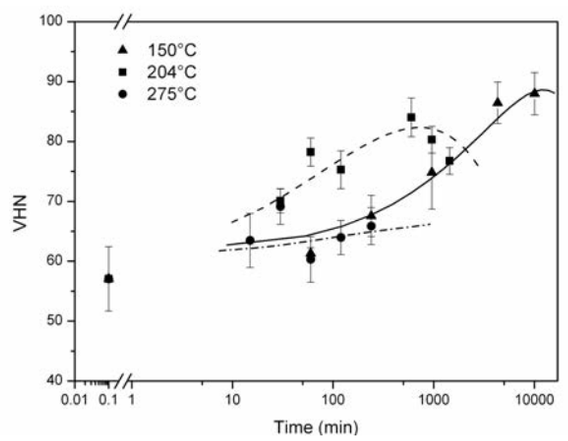


**Figure 3. Microhardness evolutions on ageing at 150°C (triangles), 204°C (squares) and 275°C (dots). The error bars are reported as the standard deviation of the measured indentations.**

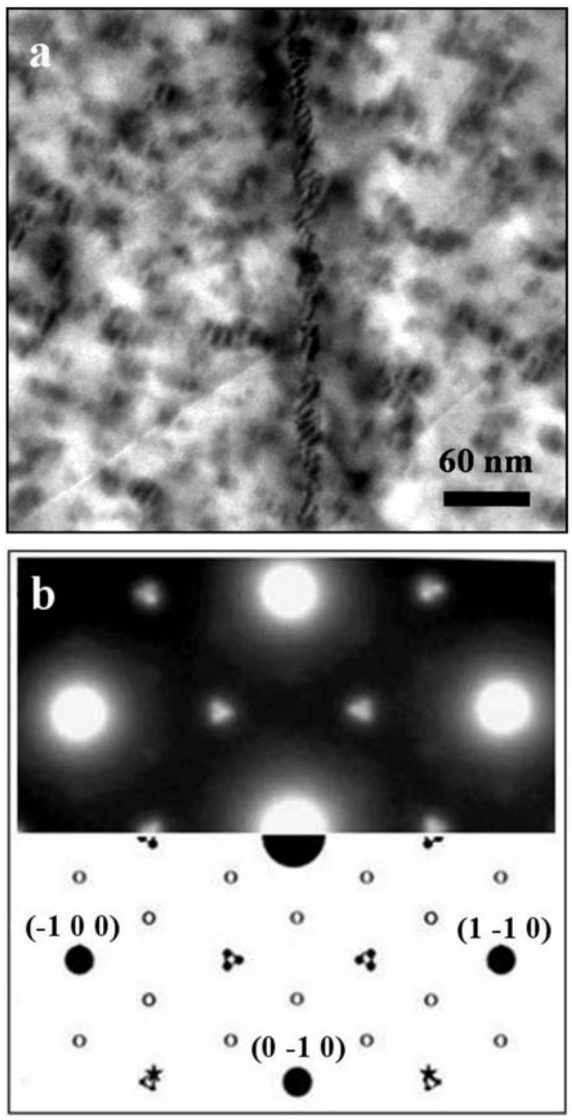


**Figure 4. Sample aged 10 h at 204 °C (T6) observed in $<001>_{Mg}$ zone axis orientation: (a) bright field, (b) SAD pattern (upper part) and SAD pattern simulation (lower part): large solid dots - Mg, open dots - $\gamma$ phase, small solid dots - double diffraction, solid stars - $\chi$ phase.**

according to the following orientation relationships with Mg:

$$(001)_{\chi} \parallel (001)_{Mg}$$
$$[1\text{–}10]_{\chi} \parallel [110]_{Mg}$$

In the SAD pattern of Figure 4b (upper part), also faint extra spots located at $1/3\{1\text{-}10\}_{Mg}$ due to the metastable hexagonal γ phase are visible. SAD analyses performed under different crystal orientations suggest the following lattice parameters and orientation relationships of the γ precipitates with the Mg matrix:

$$a_{\gamma}=0.963 \text{ nm}$$
$$c_{\gamma}=1.035 \text{ nm}$$

$$(001)_{\gamma} \parallel (001)_{Mg}$$
$$[1\text{–}10]_{\gamma} \parallel [110]_{Mg}$$

The complete spot indexation obtained by the Crystal-KitX program considering both the χ and γ phases is reported in the lower part of Figure 4b (large solid dots - Mg, open dots - γ phase, small solid dots - double diffraction, solid stars - χ phase).

Hence, as a first consequence of the results obtained so far, one can conclude that the simultaneous presence of the χ and γ precipitates, linked to the P1 and P2 signals, is responsible for the maximum age hardening of the QE22 alloy.

As already discussed above, for a complete description of the precipitation sequence outlined in Figure 1, following the position in temperature of the calorimetric signals, two other ageing treatments were studied, at 150°C and 275°C.

The calorimetric traces of the samples aged at 150°C for different times show the permanence of the P2 signal even after 16 hours (960 minutes) of ageing and the persistence of a significant dissolution D signal up to the higher ageing times.

A bright field image taken in $<100>_{Mg}$ orientation of the sample aged 16 hours at 150 °C is reported in Figure 5. Nanometric precipitates uniformly distributed inside the grains are clearly visible. The corresponding $<100>_{Mg}$ zone axis SAD pattern (not shown here) presents extra spots only due to magnesium oxide (MgO), suggesting the absence of the γ phase, that is generally easily visible in this orientation.

On the contrary, the SAD pattern taken in <001>Mg orientation shows well defined extra spots at $\sim 1/3\{\text{-}1\text{-}10\}_{Mg}$ compatible with the presence of the χ phase, Figure 6. The ring-shaped effects are due to magnesium oxide (MgO).

In conclusion, the γ phase has not yet formed after 16 hours at 150°C, and this explains the permanence of the P2 signal in the DSC traces. The hardening increases at this ageing temperature are due to the χ phase as well as to the formation of nanosized coherent aggregates.

The calorimetric traces for the samples treated at

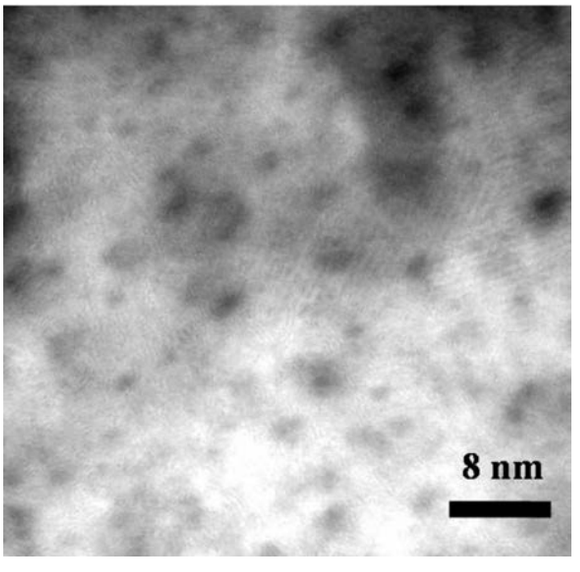


**Figure 5. Bright field image of the sample aged 16 hours at 150 °C in $<100>_{Mg}$ orientation.**

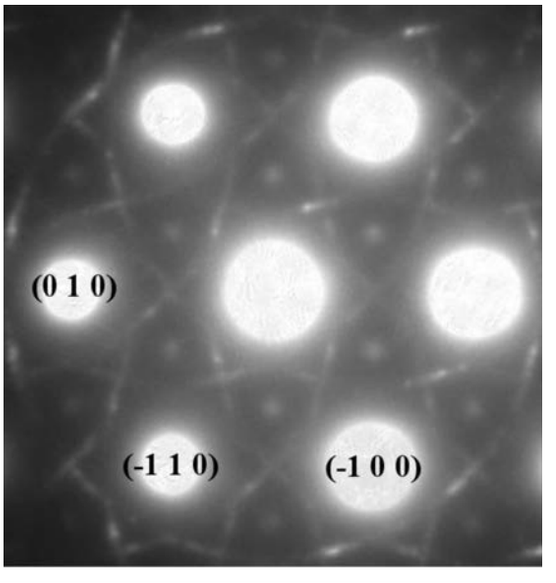


**Figure 6. SAD pattern of the sample aged 16 hours at 150°C taken in $<001>_{Mg}$ zone axis.**

275°C show that all the precipitates are already formed just after 30 minutes of ageing. TEM observations performed on samples aged at 275°C allowed to reveal the nature of the stable phase.
Figure 7 reports the main TEM results obtained for the sample aged 30 minutes at 275°C and observed in $<001>_{Mg}$ zone axis. In this sample, coarse precipitates preferentially located on dislocations and grain boundaries with dimension ranging from 30 to 170 nm, are present, Figure 7a.
The SAD pattern reported in Figure 7b (upper part) exhibits extra spots arranged in a triangular structure located at ~1/3$\{-1-10\}_{Mg}$. Although the general arrangement and the location of the spots is quite similar to those observed in the T6 sample (Figure 4b) and attributed to the $\chi$ phase, a closer look at the diffraction pattern of Figure 7b (upper part) reveals that the spots are now well separated, and their number has increased with respect to those observable in figure 4b.
The pattern simulation reported in figure 7b (lower part) allowed to attribute these extra spots to the stable $(Mg,Ag)_{12}Nd$ phase and to double diffraction effects (large solid dots - Mg, open dots - $(Mg, Ag)_{12}Nd$ phase, small solid dots - double diffraction).
Measurements carried out on the different SAD patterns, within experimental uncertainty, provide for the stable $(Mg,Ag)_{12}Nd$ phase a tetragonal structure with a=1.03 nm and c=0.59 nm, and the following orientation relationships with Mg:

$$(100)_{(Mg,Ag)12Nd} \parallel (001)_{Mg}$$
$$[0\text{-}11]_{(Mg,Ag)12Nd} \parallel [110]_{Mg}$$

All the SAD patterns taken in any other orientation are consistent with the presence of the stable $(Mg,Ag)_{12}Nd$ phase. Hence, one can conclude that the P3 signal visible in the calorimetric traces of figure 1 can be attributed to the formation of the stable $(Mg,Ag)_{12}Nd$ phase. Moreover, also the hardness trend at 275°C (Figure 3, dots and dash-dotted line), showing only a small increase during ageing, confirms the formation of the stable phase.

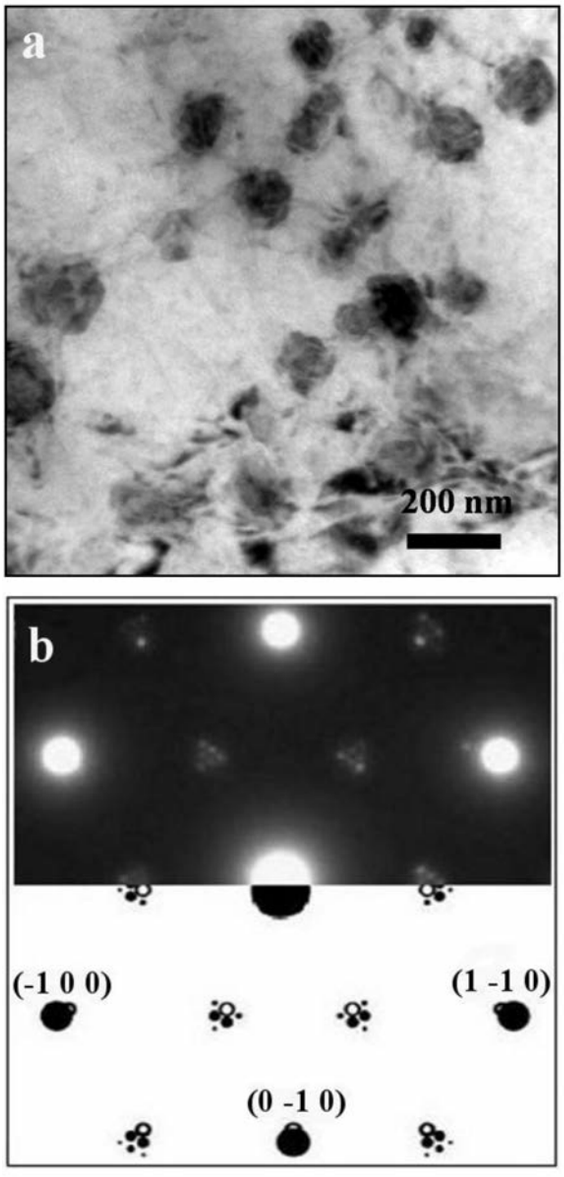


**Figure 7. Sample aged 30 min at 275°C observed in $<001>_{Mg}$ zone axis: (a) bright field image, (b) SAD pattern (upper part) and SAD pattern simulation (lower part): large solid dots - Mg, open dots - $(Mg, Ag)_{12}Nd$ phase, small solid dots - double diffraction.**

## Conclusions

The precipitation sequence responsible for the age hardening of the QE22 alloy, was studied by DSC and TEM measurements. The solution heat treated samples were submitted to thermal treatments at 150 °C, 204 °C and 275 °C for different ageing times and the results can be summarized as follows:

- the decomposition of the supersaturated solid solution occurs via the formation of nanosized coherent structures (co-clusters or GP zones) followed by the co-precipitation of two metasta-

ble hardening phases named $\chi$ and $\gamma$;
- at 150°C, the hardening increase is due to the permanence of the zones and to the precipitation of a metastable hexagonal phase, here named $\chi$;
- at the T6 (16 hours at 204°C) peak ageing condition a co-precipitation of $\chi$ and $\gamma$ occurs;
- at 275 °C, only the stable $(Mg,Ag)_{12}Nd$ phase is present, even after the shortest ageing times.

The diffraction patterns can be correctly indexed and simulated when assuming the following structures:

- an hexagonal $\chi$ phase with $a_\chi$=0.286 nm and $c_\chi$=0.521 nm and the following orientation relationships with the matrix: $(001)_\chi || (001)_{Mg}$, $[1\text{-}10]_\chi || [110]_{Mg}$.
- an hexagonal $\gamma$ phase with $a_\gamma$=0.963 nm and $c_\gamma$=1.035 nm and the following orientation relationships with the matrix: $(001)_\gamma || (001)_{Mg}$, $[100]_\gamma || [100]_{Mg}$.
- a tetragonal $(Mg,Ag)_{12}Nd$ stable phase with a=1.03 nm and c=0.59 nm and the following orientation relationships with the matrix: $(100)_{(Mg,Ag)12Nd} || (001)_{Mg}$, $[0\text{-}11]_{(Mg,\ Ag)12Nd} || [110]_{Mg}$.

## References


Barucca G, Ferragut R, Lussana D, Mengucci P, Moia F, Riontino G. Phase transformations in QE22 Mg alloy. Acta Mater 2009;57:4416-25.

CrystalKitX version 1.9.1. Total Resolution LL.

Kannan MB, Dietzel W, Blawert C, Atrensa A, Lyon P. Stress corrosion cracking of rare-earth containing magnesium alloys ZE41, QE22 and Elektron 21 (EV31A) compared with AZ80. Mater Sci Eng A 2008;480:529-39.

Lambri OA, Riehmann W. Damping due to incoherent precipitates in commercial QE22 magnesium alloy. Scripta Mater 2005;52:93-97.

Luo A, Pekguleryuz MO. Cast magnesium alloys for elevated temperature applications. J Mater Sci 1994;29:5259-71.

Payne RJM, Bailey N. Improvement of the age hardening properties of magnesium–rare earth alloys by addition of silver. J Inst Met 1959-1960;88:417.

Polmear IJ. Light alloys: from traditional alloys to nanocrystals. Elsevier, Amsterdam, 2006.

Starink MJ, Wang SC. The thermodynamics of and strengthening due to co-clusters: general theory and application to the case of Al-Cu-Mg alloys. Acta Mater 2009;57:2376-89.